

Diagnosing Critical Behavior in AdS Einstein-Maxwell-Scalar Theory via Holographic Entanglement Measures

Zhe Yang ^{1,2,*} GuangZai Ye ^{2,†} Jian-Pin Wu ^{1,‡} and Peng Liu ^{2§}

¹ *Center for Gravitation and Cosmology,*

College of Physical Science and Technology,

Yangzhou University,

Yangzhou 225009, China

² *Department of Physics and Siyuan Laboratory,*

Jinan University,

Guangzhou 510632, China

Abstract

We investigate the holographic mixed-state entanglement measures in the Einstein-Maxwell-Scalar (EMS) theory. Several quantities are computed, including the holographic entanglement entropy (HEE), mutual information (MI), entanglement wedge cross-section (EWCS), and butterfly velocity (v_B). Our findings demonstrate that these measures can effectively diagnose phase transitions. Notably, EWCS and MI, as mixed-state entanglement measures, exhibit behavior opposite to that of the HEE. Additionally, we study the butterfly velocity, a dynamic quantum information measure, and observe that it behaves differently from the static quantum information measures. We propose that the butterfly velocity is initially dominated by entanglement and subsequently by thermal entropy as the coupling constant increases. Moreover, we examine the scaling behavior of the holographic entanglement measures and find that all the critical exponents are equal to 1, which is twice that of the scalar field. We also explore the inequality between EWCS and MI, noting that the growth rate of MI consistently exceeds that of EWCS during phase transitions. These features are expected to be universal across thermodynamic phase transitions, with the inequalities becoming more significant as one moves away from the critical point.

*Electronic address: yzar55@stu2021.jnu.edu.cn

†Electronic address: photony@stu2022.jnu.edu.cn

‡Electronic address: jianpinwu@yzu.edu.cn; Corresponding author

[§]Electronic address: phylp@email.jnu.edu.cn; Corresponding author

Contents

I. Introduction	3
II. Holographic setup for Einstein-Maxwell-Scalar theory and holographic information-related quantities	5
A. The AdS Einstein-Maxwell-Scalar Model	5
B. Holographic Information-Related Quantities	6
III. The computation of holographic entanglement measures	10
A. The holographic entanglement entropy and the mutual information	10
B. The entanglement wedge cross section and the butterfly velocity	11
C. The scaling behavior of the quantum information	13
IV. The growth rate of the holographic quantum information	15
V. Discussion	18
Acknowledgments	19
References	19

I. INTRODUCTION

Quantum entanglement stands as one of the most fundamental phenomena in quantum mechanics, exhibiting properties fundamentally distinct from classical physics. Over recent years, it has become an essential tool for exploring quantum information, condensed matter physics, and quantum gravity [1–5]. Notably, quantum information measures serve as probes for phase transitions and play a pivotal role in the emergence of spacetime [6–10].

Among various quantum information measures, entanglement entropy (EE) remains the most widely used for quantifying entanglement. However, EE fails to capture mixed-state entanglement—a more common scenario than pure states. To address this limitation, alternative measures such as reflected entropy, mutual information (MI), and entanglement of purification (EOP) have been developed [11–14]. These measures have proven effective in diagnosing various phase transitions, including quantum, topological, and superconducting

transitions [1, 5, 15], revealing a deep connection between entanglement and critical phenomena. In condensed matter physics, many important phase transitions occur in strongly correlated systems—high-temperature superconductors, heavy fermions, and the fractional quantum Hall effect [16–19]. Studying entanglement in these systems remains exceptionally challenging, necessitating novel theoretical approaches.

The gauge/gravity duality has emerged over the past two decades as a powerful framework for studying strongly correlated systems [20, 21]. Within this framework, a strongly correlated quantum system maps to a classical gravitational theory, enabling the construction of holographic duals for various entanglement measures. The most prominent example is holographic entanglement entropy (HEE), corresponding to the minimal surface area in the bulk [2]. HEE has been extensively applied to probe thermodynamic and quantum phase transitions [22–30]. More recently, the entanglement wedge cross-section (EWCS) was introduced as a novel measure [31, 32], serving as the holographic dual of reflected entropy, logarithmic negativity, and balanced partial entanglement [33–36]. Studies have demonstrated that EWCS provides a robust measure of mixed-state entanglement [22, 30, 37–42]. Beyond these static measures, the butterfly velocity v_B captures the dynamical spread of quantum information and characterizes chaos in the system [43]. This dynamical probe has been studied across various holographic models [44–48], complementing the static entanglement measures in characterizing phase transitions.

The Einstein-Maxwell-Scalar (EMS) theory represents a paradigmatic holographic model exhibiting spontaneous scalarization as temperature or coupling constant varies. Upon crossing the critical point, the system undergoes a phase transition from the normal to the scalarized state. While extensive studies have examined HEE in this context, a comprehensive analysis of EWCS as a mixed-state entanglement probe remains absent. Our previous work on holographic p-wave superconductors revealed an inequality between the growth rates of EWCS and MI [38], raising the question of whether this inequality persists in the EMS theory. Furthermore, butterfly velocity—as a dynamical quantum information measure—exhibits distinct behavior from static measures like HEE and EWCS. Since HEE receives significant contributions from thermal entropy in mixed-state systems while EWCS more faithfully captures quantum correlations, understanding the behavior of v_B in this context fills a critical gap. This paper presents a systematic investigation of holographic entanglement measures in EMS theory.

This paper is organized as follows. In Section II, we introduce the EMS model and the relevant holographic quantum information measures: HEE, MI, EWCS, and butterfly velocity. Section III presents numerical results and analyzes the scaling behavior of these measures. In Section IV, we examine the inequality between the growth rates of MI and EWCS. We conclude with a summary and outlook in Section V.

II. HOLOGRAPHIC SETUP FOR EINSTEIN-MAXWELL-SCALAR THEORY AND HOLOGRAPHIC INFORMATION-RELATED QUANTITIES

A. The AdS Einstein-Maxwell-Scalar Model

The action of the Einstein-Maxwell-scalar theory in the AdS spacetime is [49, 50],

$$S = \int d^4\sqrt{-g} \left[R + \frac{6}{L^2} - \nabla_\mu \phi \nabla^\mu \phi - \frac{1}{2} f(\phi) F_{\mu\nu} F^{\mu\nu} \right], \quad (1)$$

where R is Ricci scalar, L is the AdS length scale, and ϕ is a real scalar field. A_μ is the gauge field and the field strength $F_{\mu\nu} = \nabla_\mu A_\nu - \nabla_\nu A_\mu$. $f(\phi)$ is the coupling function between electromagnetic and scalar fields. In this paper, we define it is $f(\phi) = e^{-b\phi^2}$ and b is a dimensionless coupling constant. The equation of motion (EOM) of this action is,

$$R_{\mu\nu} - \frac{1}{2} R g_{\mu\nu} - \frac{3}{L^2} g_{\mu\nu} = T_{\mu\nu}^\phi + f(\phi) T_{\mu\nu}^A, \quad (2)$$

$$\nabla_\mu \nabla^\mu \phi = \frac{1}{4} \frac{df(\phi)}{d\phi} F_{\mu\nu} F^{\mu\nu}, \quad (3)$$

$$\nabla_\mu (f(\phi) F^{\mu\nu}) = 0, \quad (4)$$

where the energy-momentum tensor

$$T_{\mu\nu}^\phi = \nabla_\mu \phi \nabla_\nu \phi - \frac{1}{2} g_{\mu\nu} \nabla_\rho \phi \nabla^\rho \phi, \quad (5)$$

$$T_{\mu\nu}^A = F_{\mu\rho} F^\rho_\nu - \frac{1}{4} g_{\mu\nu} F_{\rho\sigma} F^{\rho\sigma}. \quad (6)$$

We solve the EOM with this ansatz,

$$ds^2 = \frac{1}{z^2} \left(-(1-z)p(z)U(z)dt^2 + \frac{dz^2}{(1-z)p(z)U(z)} + V(z)(dx^2 + dy^2) \right), \quad (7)$$

$$A_\mu = \mu(1-z)a(z)dt. \quad (8)$$

where μ is the chemical potential of gauge field and $p(z) = 1 + z + z^2 - \mu^2 z^3/2$. We set $z = r_h/r$, where the radial coordinate z ranges from 0 to 1, with $z = 0$ representing the AdS

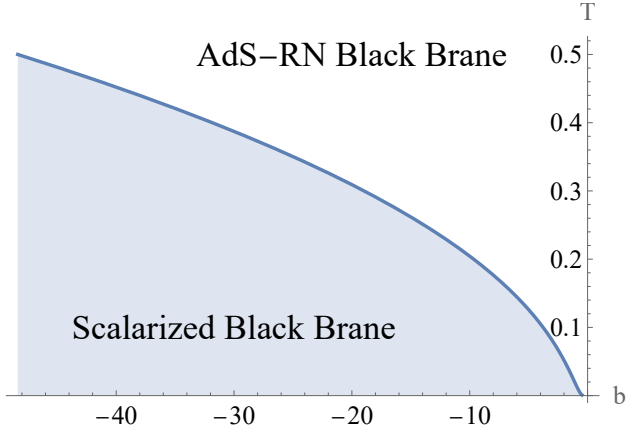


Fig. 1. Phase diagram of thermal phase transition in the EMS model.

boundary and $z = 1$ representing the horizon. The quantities U, V, a, ϕ are the functions of z , which can be obtained by solving the EOM. Additionally, the ansatz will return to AdS-RN black brane when we set $a = U = V = 1$, and $\phi = 0$.

The Hawking temperature of this system is given by $\tilde{T} = \frac{6-\mu^2}{8\pi}$. Notably, the system remains invariant under the following rescaling:

$$\begin{aligned} (t, x, y) &\rightarrow \alpha^{-1}(t, x, y), & V &\rightarrow \alpha^2 V, \\ \mu &\rightarrow \alpha\mu, & \tilde{T} &\rightarrow \alpha\tilde{T}. \end{aligned} \tag{9}$$

In this paper, we set μ as the scaling unit, making the dimensionless Hawking temperature $T = \tilde{T}/\mu$. It is evident that by varying the coupling constant b and the Hawking temperature T , the system transitions from an AdS-RN black brane to a scalarized black hole. The phase transition of this system is illustrated in Fig. 1.

B. Holographic Information-Related Quantities

Quantum entanglement fundamentally distinguishes quantum from classical physics. Among the various measures of entanglement, entanglement entropy (EE) stands out as the most widely adopted. For a density matrix ρ_A , EE is defined as [51]

$$\rho_A = \text{Tr}_B(\rho), \quad S_A = -\text{Tr}(\rho_A \log \rho_A). \tag{10}$$

In the holographic framework, the EE of a boundary region A equals the area of the corresponding minimal surface in the bulk—the holographic entanglement entropy (HEE), illus-

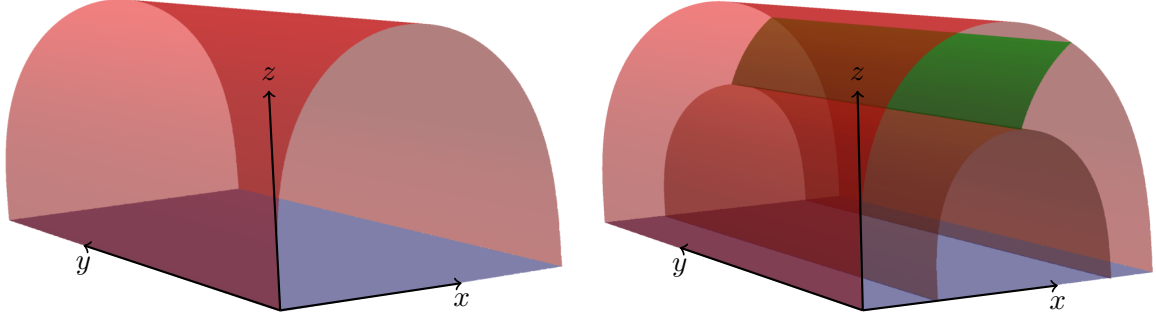


Fig. 2. The left plot: The minimum surface for a given width w . The right plot: The minimum cross-section (green surface) of the entanglement wedge.

trated in the left plot of Fig. 2. Specifically,

$$S_A = \frac{\gamma_A}{4G_N}. \quad (11)$$

where G_N is the Newton constant and γ_A is the area of the minimal surface that corresponds to the region A on the boundary [2].

We consider an infinite strip along the y -direction in a homogeneous background geometry:

$$ds^2 = g_{tt}dt^2 + g_{zz}dz^2 + g_{xx}dx^2 + g_{yy}dy^2. \quad (12)$$

As illustrated in Fig. 2, the minimal surface area depends on the strip width w :

$$A_{\gamma_A} = L_y \int_0^w \sqrt{g_{yy}(g_{xx} + g_{zz}z'(x)^2)} dx, \quad (13)$$

where $L_y = \int dy$ and the strip width is $w = \int dx$. For an infinite strip along the y -direction, L_y factors out. Minimizing (13) via the Euler-Lagrange equation yields

$$2g_{yy}g_{zz}z'(x)^2g'_{xx} + g_{xx}(g_{yy}(-2g_{zz}z''(x) - z'(x)^2g'_{zz} + g'_{xx}) + g_{zz}z'(x)^2g'_{yy}) + g_{xx}^2g'_{yy} = 0. \quad (14)$$

This equation enables numerical computation of the HEE [29]. However, in mixed-state systems, HEE receives substantial contributions from thermal entropy [24], motivating the search for alternative entanglement measures.

Mutual information (MI) provides a more suitable measure for mixed-state entanglement [11, 14]. Unlike EE, which remains nonzero even for unentangled product states $\mathcal{H}_A \otimes \mathcal{H}_B$, MI vanishes for such states by construction. We consider a bipartite system with subsystems a and c separated by region p (Fig. 3). The holographic MI reads [52]

$$I(a, c) = S(a) + S(c) - \min(S(a \cup c)). \quad (15)$$

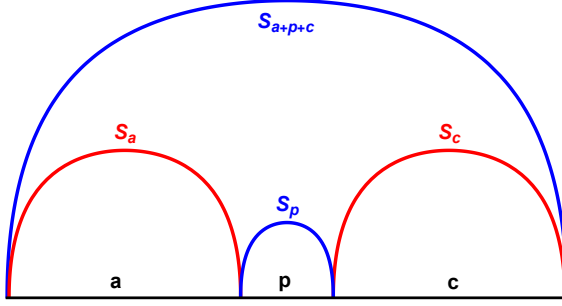


Fig. 3. The Illustration of holographic mutual information.

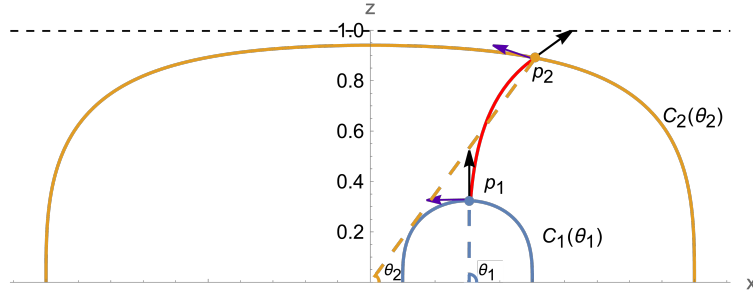


Fig. 4. The illustration depicting the calculation of EWCS, and the red surface representing the minimum cross-section.

where $S(a)$ and $S(c)$ denote the HEE of subsystems a and c , respectively. A positive MI signals entanglement; zero or negative values indicate a disentangled phase where thermal effects dominate. Nevertheless, MI can still be influenced by thermal entropy in certain configurations [30], prompting interest in additional mixed-state measures.

The EWCS has emerged as a promising mixed-state entanglement measure [31, 32], defined as the minimal cross-sectional area within the entanglement wedge (right plot of Fig. 2). It serves as the holographic dual of various quantum information measures [33–35]:

$$E_W(\rho_{ab}) = \min_{\Sigma_{ab}} \left(\frac{\text{Area}(\Sigma_{ab})}{4G_N} \right). \quad (16)$$

However, the calculation of EWCS remains challenging. There are several difficulties in calculating EWCS. First, the EOM for the minimum surface in the EWCS are highly nonlinear, making them difficult to solve. Second, finding the minimum surface is essentially a quadratic minimization problem, as the EWCS represents a global minimum cross-section located on the minimum surface within the entanglement wedge. This makes the search for the global minimum cross-section particularly challenging. Third, the coordinates near the

AdS boundary ($z \rightarrow 0$) are singular, requiring high numerical precision to ensure accuracy.

Next, we will briefly introduce the algorithm for calculating the EWCS, particularly for the asymmetric EWCS, which involves more diverse configurations [29]. In this paper, we consider a bipartite system $a \cup c$ divided by region p . It should be noted that EWCS exists only when the MI is greater than zero. As illustrated in Fig. 4, the minimum surfaces of regions c and $a+p+c$ can be represented as $(C_1(\theta_1), C_2(\theta_2))$, respectively. The cross-section intersects these minimum surfaces at points p_1 and p_2 , and the area of the cross-section can be calculated as follows:

$$A = \int_{C_{p_1, p_2}} \sqrt{g_{xx}g_{yy}x'(z)^2 + g_{zz}g_{yy}} dz. \quad (17)$$

Variating the (17), we can obtain the EOM of the cross-section is

$$x'(z)^3 \left(\frac{g_{xx}g'_{yy}}{2g_{yy}g_{zz}} + \frac{g'_{xx}}{2g_{zz}} \right) + x'(z) \left(\frac{g'_{xx}}{g_{xx}} + \frac{g'_{yy}}{2g_{yy}} - \frac{g'_{zz}}{2g_{zz}} \right) + x''(z) = 0. \quad (18)$$

It needs to be noted that the global minimum cross-section is orthogonal to the entanglement wedge, which implies that

$$\left\langle \frac{\partial}{\partial z}, \frac{\partial}{\partial \theta_1} \right\rangle_{p_1} = 0, \quad \left\langle \frac{\partial}{\partial z}, \frac{\partial}{\partial \theta_2} \right\rangle_{p_2} = 0 \quad (19)$$

where $\langle \cdot, \cdot \rangle$ represents the vector product with metric $g_{\mu\nu}$. We can normalize the orthogonal relation,

$$Q_1(\theta_1, \theta_2) \equiv \left. \frac{\langle \frac{\partial}{\partial z}, \frac{\partial}{\partial \theta_1} \rangle}{\sqrt{\langle \frac{\partial}{\partial z}, \frac{\partial}{\partial z} \rangle \langle \frac{\partial}{\partial \theta_1}, \frac{\partial}{\partial \theta_1} \rangle}} \right|_{p_1} = 0, \quad Q_2(\theta_1, \theta_2) \equiv \left. \frac{\langle \frac{\partial}{\partial z}, \frac{\partial}{\partial \theta_1} \rangle}{\sqrt{\langle \frac{\partial}{\partial z}, \frac{\partial}{\partial z} \rangle \langle \frac{\partial}{\partial \theta_2}, \frac{\partial}{\partial \theta_2} \rangle}} \right|_{p_2} = 0. \quad (20)$$

The cross-section endpoints lie on the two minimal surfaces $(C_1(\theta_1), C_2(\theta_2))$ at parameters (θ_1, θ_2) . Imposing the boundary conditions (20) locates the global minimum; we employ the Newton-Raphson method to find (θ_1, θ_2) and thereby compute the asymmetric EWCS.

Unlike the static measures discussed above, the butterfly velocity v_B captures the dynamical spread of quantum information. It quantifies the speed of chaos propagation in many-body systems and, in the holographic picture, is determined by localized shockwaves on the black hole horizon [44, 45]. This dynamical quantity encodes the spreading and causal structure of the system, revealing deep connections between entanglement and geometry. For general anisotropic black branes [47],

$$v_B = \sqrt{\left. \frac{-2\pi T \mu V_y(z)}{V_y(z)(V'_x(z) - 2V_x(z)) + V_x(z)(V'_y(z) - 2V_y(z))} \right|_{z=1}}. \quad (21)$$

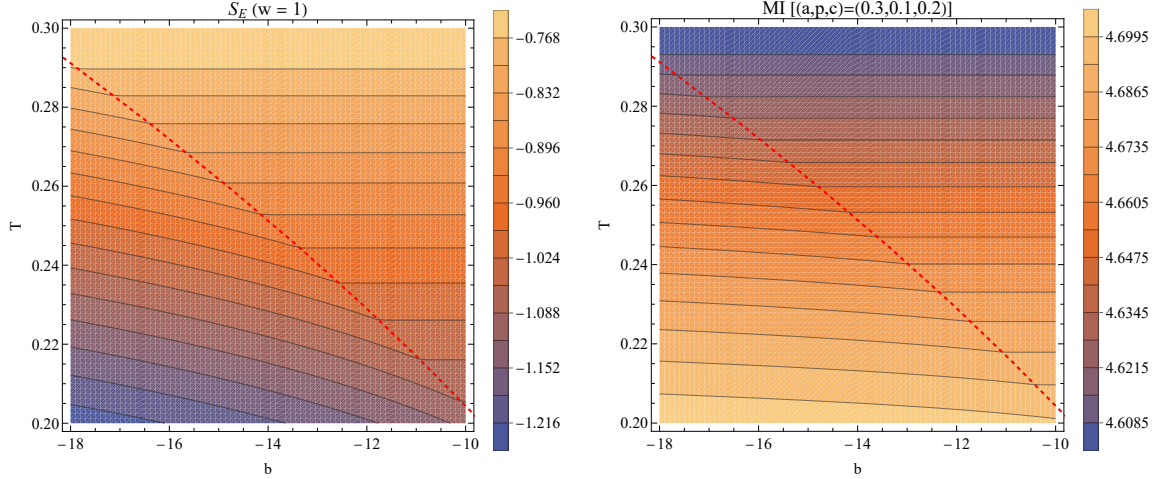


Fig. 5. The behavior of HEE and MI versus temperature T and coupling constant b when the phase transition occurs. The red dashed line represents the critical point. Left plot: the behavior of HEE S_E when we set the width $w = 1$. Right plot: the behavior of MI when we set the configurations $(a, p, c) = (0.3, 0.1, 0.2)$.

For an isotropic EMS model, this simplifies to

$$v_B = \sqrt{\left. \frac{\pi T \mu}{2V(z) - V'(z)} \right|_{z=1}}. \quad (22)$$

Thus v_B depends on the Hawking temperature T , chemical potential μ , and background geometry $V(z)$, enabling a direct comparison with static entanglement measures across the phase transition.

III. THE COMPUTATION OF HOLOGRAPHIC ENTANGLEMENT MEASURES

With the holographic setup established in the previous section, we now present the numerical results for various entanglement measures and analyze their behavior during the phase transition.

A. The holographic entanglement entropy and the mutual information

The left plot of Fig. 5 displays the HEE behavior across the phase transition. HEE effectively signals the transition: it decreases sharply as the coupling constant b diminishes and the scalarized solution emerges, with a similar sharp drop as temperature T falls through the

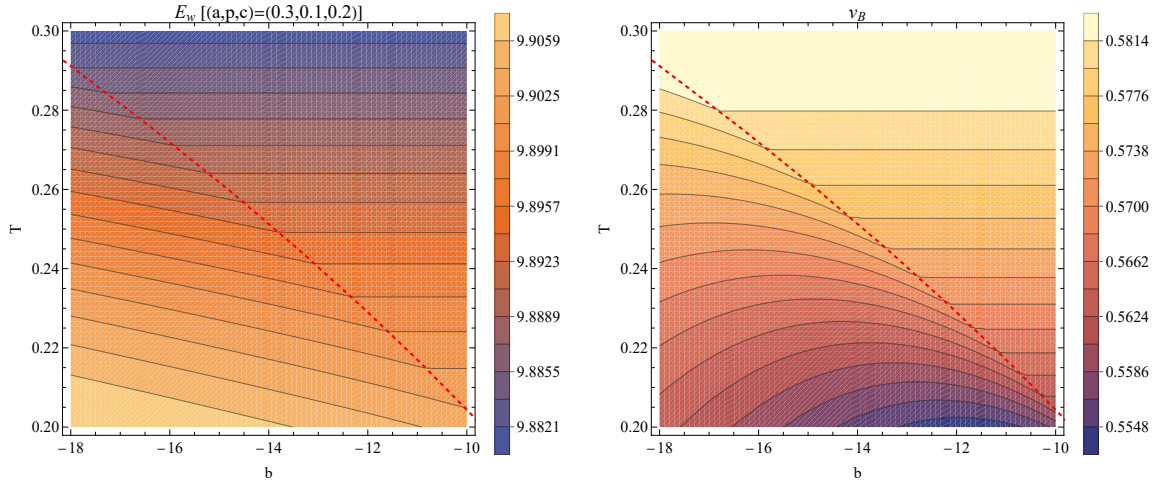


Fig. 6. The red dashed line represents the critical point of the phase transition. Left plot: the behavior of EWCS E_w versus different coupling constant b and the temperature T . Right plot: the behavior of butterfly velocity v_B versus different coupling constant b and the temperature T .

critical point. The rate of change accelerates markedly in the scalarized phase. However, for large strip widths, HEE becomes dominated by thermal entropy [24, 25]—consistent with the parallel behavior of HEE and thermal entropy as T decreases in EMS theory. This thermal contamination limits the utility of HEE for probing genuine mixed-state entanglement, motivating the use of alternative measures.

The right plot of Fig. 5 shows MI behavior during the transition. In stark contrast to HEE, MI increases as b decreases and rises sharply at the critical point; it also grows with decreasing T . This opposite trend suggests that MI better captures the quantum correlations enhanced during the transition. Nevertheless, in certain configurations MI remains influenced by thermal contributions [30], warranting examination of additional mixed-state measures.

Having examined the static entanglement measures HEE and MI, we now turn to EWCS and the dynamical measure, butterfly velocity v_B .

B. The entanglement wedge cross section and the butterfly velocity

The left plot of Fig. 6 presents the EWCS behavior. Like MI, EWCS increases as b decreases and as T drops, exhibiting behavior opposite to HEE. This confirms that both MI

and EWCS, as mixed-state measures, capture aspects of entanglement that HEE misses.

The right plot reveals strikingly different behavior for the dynamical measure v_B . Unlike the monotonic trends of static measures, v_B displays non-monotonic behavior with respect to b : it first decreases then increases as b diminishes. In contrast, v_B decreases monotonically with temperature. This non-monotonicity arises from competing contributions in Eq. (22). Specifically,

$$v_B \propto \frac{1}{2V(z) - V'(z)} \Big|_{z=1}. \quad (23)$$

The two terms in Eq. (23) encode distinct physics. The thermal entropy density is

$$s = \frac{2\pi A}{\kappa} = \frac{2\pi V(z)}{\kappa} \hat{V} \Big|_{z=1}, \quad (24)$$

where A represents the area of the horizon and $\hat{V} = \int dx dy$ denotes the area of the corresponding region of the dual system. Consequently, the first term $V(z)$ in (23) is associated with the thermal entropy of the system. Moreover, when considering the symmetric EWCS and combining (17) with the ansatz (8), the expression for the E_w integral can be expanded as follows,

$$E_w = \int_{\Sigma} \left(\frac{g_{zz}(z)V'(z) + V(z)g'_{zz}(z)}{4\sqrt{V(z)g_{zz}(z)}} (z-1)^2 + \mathcal{O}(z-1)^3 \right) dz. \quad (25)$$

Therefore, we find that EWCS, as a novel measure of mixed-state entanglement, is given by $E_w \propto V'(z)$, which corresponds to the second term in (23).

The left plot of Fig. 7 shows that $2V(z) - V'(z)$ exhibits non-monotonic behavior due to competition between its two terms. As b decreases, $V'(z)$ initially dominates, causing the function to increase; beyond the peak, $2V(z)$ takes over and the function decreases.

The right plot of Fig. 7 illustrates how this competition shapes v_B . The decreasing portion of v_B is governed by $V'(z)$, linked to mixed-state entanglement, while the ascending portion reflects the dominance of $V(z)$, associated with thermal entropy (cf. Eq. (24)).

In summary, v_B exhibits non-monotonic behavior because entanglement-related and thermal contributions compete: the former dominates initially as b decreases, yielding a decrease in v_B , while the latter takes over near the critical point, causing v_B to rise. This intrinsic competition distinguishes the dynamical measure v_B from static entanglement probes and should manifest in other phase transitions as well.

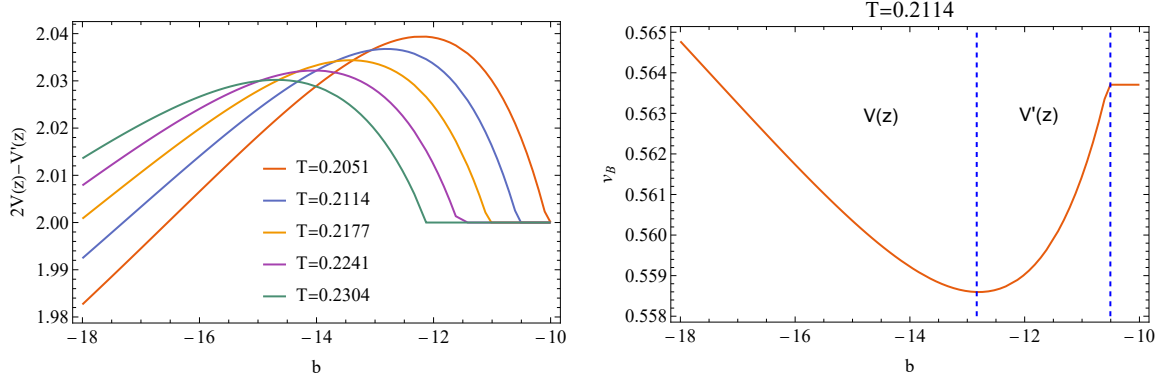


Fig. 7. Left plot: the function $(2V(z) - V'(z))|_{z=1}$ versus the coupling constant b at different temperatures T . Right plot: the butterfly velocity v_B versus b at $T = 0.2114$. The blue dashed line represents the peak point of v_B and the critical point, respectively. As the coupling constant b decreases, the region of v_B is predominantly influenced by $V'(z)$ and $V(z)$, respectively.

The above analysis reveals distinct behaviors of various entanglement measures during the phase transition. To gain deeper insights into their universal properties, we now investigate their scaling behavior near the critical point.

C. The scaling behavior of the quantum information

The critical point in EMS theory marks a second-order phase transition from the normal to the scalarized state. Universality dictates that diverse physical systems share similar scaling behaviors near criticality, making the extraction of critical exponents a valuable diagnostic. We define the difference between scalarized and normal phases:

$$\delta v_B = v_B^{\text{scalar}} - v_B^{\text{normal}}, \quad S_E = S_E^{\text{scalar}} - S_E^{\text{normal}}, \quad \delta E_w = E_w^{\text{scalar}} - E_w^{\text{normal}}. \quad (26)$$

Therefore, the critical behavior for the butterfly velocity, HEE, and EWCS can be read as

$$\delta v_B \sim \left(1 - \frac{T}{T_c}\right)^{\alpha_{v_B}}, \quad \delta S_E \sim \left(1 - \frac{T}{T_c}\right)^{\alpha_{S_E}}, \quad \delta E_w \sim \left(1 - \frac{T}{T_c}\right)^{\alpha_{E_w}}, \quad (27)$$

The critical exponents α_{v_B} , α_{S_E} , and α_{E_w} characterize the scaling of v_B , HEE, and EWCS, respectively. Figure 8 displays the scaling of v_B with both T and b ; the slope yields the critical exponent. We find

$$\alpha_{v_B}^T \approx \alpha_{v_B}^b \approx 1. \quad (28)$$

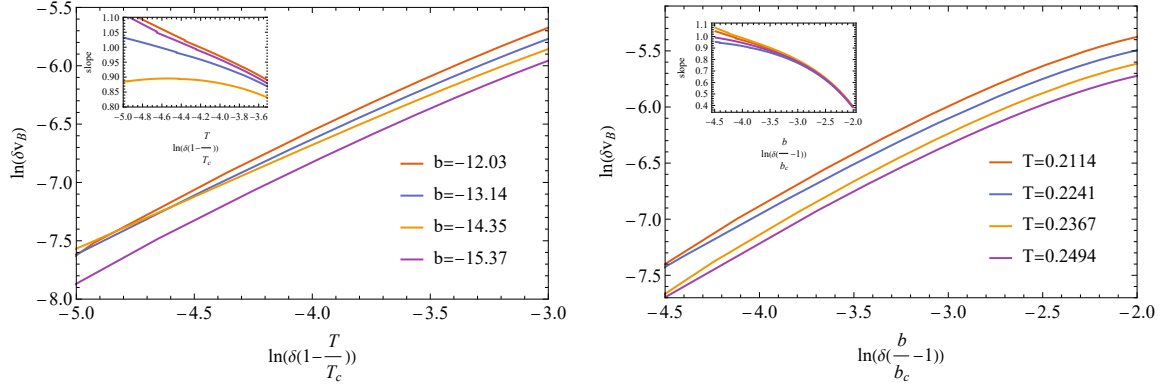


Fig. 8. The scaling behavior of butterfly velocity v_B . The inset plot is the slope of the scaling behavior, which represents the critical exponent. Left plot: the scaling behavior of v_B with the change of temperature T . Right plot: the scaling behavior of v_B with the change of coupling constant b , where b_c represents the critical coupling constant.

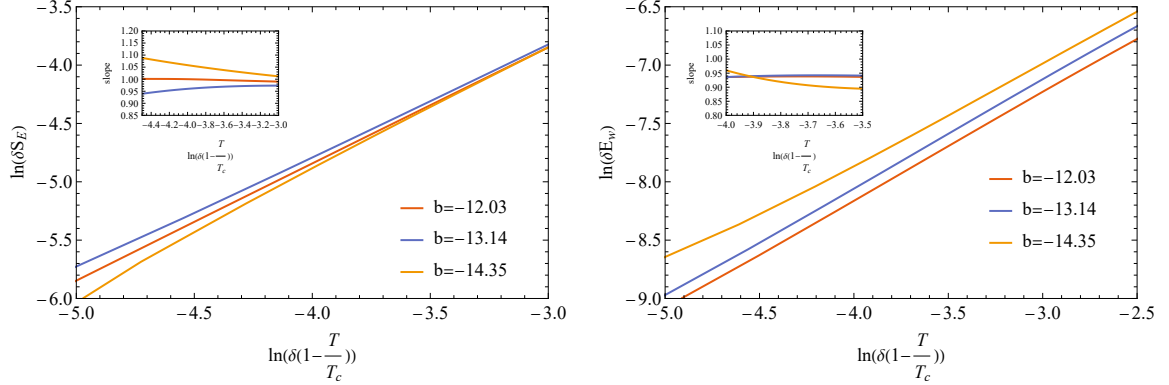


Fig. 9. The scaling behavior of HEE S_E and EWCS E_w . The inset plot is the slope of the scaling behavior, which represents the critical exponent. Left plot: the scaling behavior of S_E with the change of temperature. Right plot: the scaling behavior of E_w with the change of temperature.

In Fig. 9, we illustrate the scaling behavior of both the HEE and the EWCS. It is important to note that both the dynamic quantum information and the static quantum information, exhibit similar critical exponents. Our numerical results indicate that,

$$\alpha_{v_B} \approx \alpha_{S_E} \approx \alpha_{E_w} \approx 1. \quad (29)$$

To better investigate why all holographic quantum information exhibit the same critical

exponent, we study the scaling behavior of the scalar field ϕ . The expansion of ϕ near the AdS boundary is given by [50],

$$\phi = z^3\phi_3 + \mathcal{O}(z^4). \quad (30)$$

We show the scaling behavior of the ϕ_3 in Fig. 10. Our numerical result shows that the scaling behavior of the ϕ_3 with temperature and coupling constant is

$$\delta(\phi_3) \sim (1 - \frac{T}{T_c})^{\alpha_\phi^T} \sim (\frac{b}{b_c} - 1)^{\alpha_\phi^b}, \quad (31)$$

where the critical exponent $\alpha_\phi^T = \alpha_\phi^b = 1/2$. It is important to note that the critical exponent of other holographic quantum information is always twice that of ϕ_3 ,

$$\alpha_{v_B} = \alpha_{S_E} = \alpha_{E_w} = 2\alpha_\phi^T = 2\alpha_\phi^b. \quad (32)$$

We can consider $\delta\phi_3$ as the perturbation when the phase transition occurs. Near the critical point, we can expand the scalar field and metric function as follows [53, 54],

$$\begin{aligned} \phi &= \epsilon\phi_1 + \epsilon^3\phi_2 + \epsilon^5\phi_3 + \dots, \\ U &= 1 + \epsilon^2U_2 + \epsilon^4U_3 + \dots, \\ V &= 1 + \epsilon^2V_2 + \epsilon^4V_3 + \dots. \end{aligned} \quad (33)$$

we can find the perturbation of the metric function is twice than the scalar field,

$$\delta g_{\mu\nu} \sim (\delta\phi)^2. \quad (34)$$

Therefore, we can conclude that the critical exponents of geometry-related quantities are always twice that of the scalar field.

Beyond the individual behavior of each entanglement measure, we are particularly interested in the relative growth rates of MI and EWCS, which may reveal universal features of thermodynamic phase transitions.

IV. THE GROWTH RATE OF THE HOLOGRAPHIC QUANTUM INFORMATION

Inequalities between different holographic quantum information have been widely studied, such as the inequality $E_w(\rho_{AC}) \geq \frac{1}{2}I(A, C)$ [55]. These inequalities can deepen our understanding of the properties of mixed-state entanglement measures. In our previous

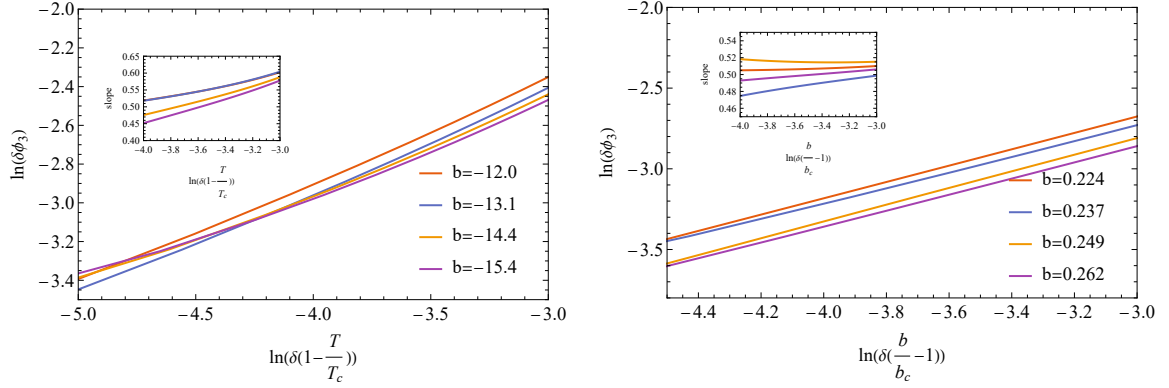


Fig. 10. The scaling behavior of ϕ_3 . The inset plot represents the slope of the scaling behavior, which can represent the critical exponent. Left plot: the scaling behavior of ϕ_3 as a function of temperature. Right plot: the scaling behavior of ϕ_3 with respect to the coupling constant b .

study, we have found an inequality between the growth rate of the EWCS and the MI in the holographic p-wave superconductor [38]. We found that the growth rate of MI near the critical point is always greater than that of EWCS. We propose that this inequality is linked to the definition of holographic quantum information. However, the EMS theory differs from the holographic superconductor theory, and the coupling constant b also influences the phase transition. Therefore, it is necessary to investigate whether the inequality still holds in this theory, which could help broaden the scope of where such an inequality occurs.

When the temperature or coupling constant crosses the critical point, the system occurs the phase transition from the normal state to the scalarized state. To better investigate the growth rate of the holographic quantum information, we define the relative values of the MI and the EWCS as follows:

$$\tilde{I} = \frac{I_{\text{scalar}}}{I_{\text{norm}}}, \quad \tilde{E}_w = \frac{E_{w,\text{scalar}}}{E_{w,\text{norm}}}. \quad (35)$$

With this definition, we can fix \tilde{E}_w and \tilde{I} to 1 at the critical point. As the temperature or the coupling constant changes, the relative values of MI and EWCS begin to change rapidly. Near the critical point, the behavior of these relationships can be described as follows:

$$\delta(Q) \sim A(Q)(1 - \frac{T}{T_c})^\alpha, \quad (36)$$

where Q is any physical quantity occurs critical behaviors. Therefore, EWCS and MI can

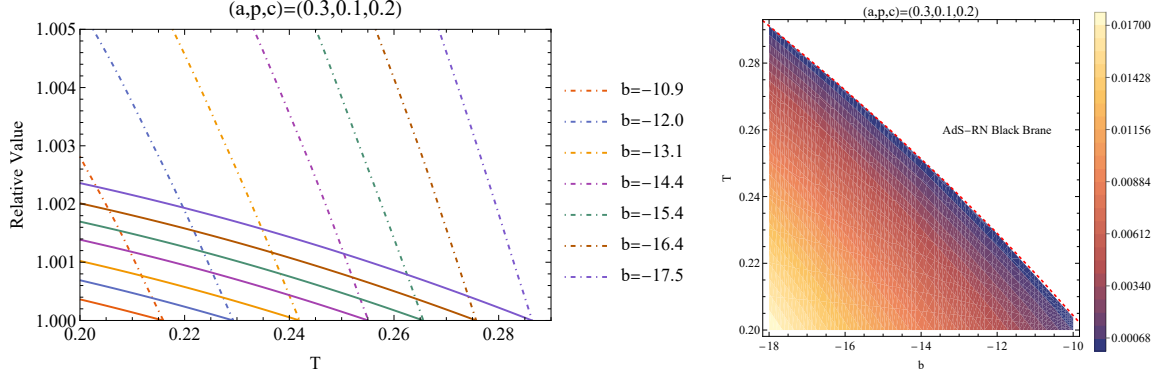


Fig. 11. The growth rate of EWCS and MI with the same configuration. Left plot: the relative values of EWCS and MI with varying coupling constants b , at the phase transition point. The solid line represents the relative value of EWCS \tilde{E}_w . The dashed line represents the relative value of MI \tilde{I} . Right plot: the value of $A(\tilde{I}) - A(\tilde{E}_w)$. The red dashed line marks the critical point of the phase transition.

be represent as,

$$\tilde{E}_w = 1 + A(\tilde{E}_w) \left(1 - \frac{T}{T_c}\right)^\alpha, \quad \tilde{I} = 1 + A(\tilde{I}) \left(1 - \frac{T}{T_c}\right) \quad (37)$$

It is easy to observe that $A(Q)$ measures the increasing behavior of holographic quantum information, which allows us to refer to A as the growth rate. In the left plot of Fig. 11, we present the relative values of EWCS and MI at the phase transition. We find that the relative value of MI increases quickly than that of EWCS, indicating that the growth rate of MI is higher than EWCS,

$$A(\tilde{I}) \geq A(\tilde{E}_w). \quad (38)$$

To better investigate this inequality in holographic quantum information, we show the value of $A(\tilde{I}) - A(\tilde{E}_w)$ in the right plot of Fig. 11. We find that whenever the phase transition occurs, either with respect to temperature T or the coupling constant b , the inequality is consistently validated. Additionally, as move away from the critical point, the inequality becomes more significant. Therefore, we propose that this inequality is closely related to the thermodynamic phase transition. Based on our previous investigation of the holographic p-wave superconductor [38], we demonstrate that this inequality generally holds within this class of theories. This inequality appears in the system whenever a thermodynamic phase transition occurs. We suggest that this inequality is associated with the properties

of holographic quantum information. MI measures the total correlation of the system, which comprises both quantum and classical correlations. On the other hand, EWCS is considered as the holographic dual of several different mixed-state entanglement measures, only captures part of the correlation within the system. Therefore, when the phase transition occurs, despite having the same configuration, MI can capture more information than EWCS, making it more significant in diagnosing the phase transition.

This inequality deepens our understanding of the relationship among holographic entanglement measures and provides a window into the universal features of thermodynamic phase transitions.

V. DISCUSSION

We have systematically investigated holographic entanglement measures in EMS theory, encompassing both static probes (HEE, MI, EWCS) and the dynamical butterfly velocity v_B . All measures effectively diagnose the phase transition, yet they exhibit qualitatively distinct behaviors. While HEE decreases with both decreasing temperature and coupling constant, the mixed-state measures MI and EWCS increase—highlighting their complementary sensitivity to quantum correlations. The butterfly velocity v_B behaves differently still: it varies monotonically with temperature but non-monotonically with the coupling constant. This non-monotonicity reflects a competition between contributions linked to entanglement ($V'(z)$) and thermal entropy ($V(z)$), offering insight into how dynamical measures probe phase transitions.

We also examined the scaling behavior near criticality. All entanglement measures share a universal critical exponent $\alpha = 1$, precisely twice that of the scalar order parameter ($\alpha_\phi = 1/2$). This doubling arises because the entanglement measures depend quadratically on the scalar field. Furthermore, we identified an inequality between the growth rates of MI and EWCS: MI consistently grows faster than EWCS during the transition. Since MI captures total correlations while EWCS measures only a subset, this hierarchy appears intrinsic to holographic systems and should persist across thermodynamic phase transitions.

Looking ahead, extending this analysis to other phase transitions—topological, quantum, and in alternative gravity theories [56–66]—presents a natural next step. In particular, it remains an open question whether the MI–EWCS inequality holds for quantum phase

transitions, whose underlying mechanisms differ fundamentally from thermodynamic ones.

Acknowledgments

Peng Liu would like to thank Yun-Ha Zha, Yi-Er Liu and Bai Liu for their kind encouragement during this work. Zhe Yang appreciates Feng-Ying Deng's support and warm words of encouragement during this work. We are also very grateful to Chong-Ye Chen for their helpful discussion and suggestions. This work is supported by the Natural Science Foundation of China under Grant Nos. 12475054, 12375055 and the Guangdong Basic and Applied Basic Research Foundation No. 2025A1515012063. Zhe Yang is supported by the Jiangsu Postgraduate Research and Practice Innovation Program under Grant No. KYCX25_3922.

- [1] A. Osterloh, L. Amico, G. Falci and R. Fazio, “Scaling of entanglement close to a quantum phase transition,” *Nature* **416**, no.6881, 608-610 (2002) doi:10.1038/416608a
- [2] S. Ryu and T. Takayanagi, “Holographic derivation of entanglement entropy from AdS/CFT,” *Phys. Rev. Lett.* **96**, 181602 (2006) doi:10.1103/PhysRevLett.96.181602 [arXiv:hep-th/0603001 [hep-th]].
- [3] A. Lewkowycz and J. Maldacena, “Generalized gravitational entropy,” *JHEP* **08**, 090 (2013) doi:10.1007/JHEP08(2013)090 [arXiv:1304.4926 [hep-th]].
- [4] V. E. Hubeny, M. Rangamani and T. Takayanagi, “A Covariant holographic entanglement entropy proposal,” *JHEP* **07**, 062 (2007) doi:10.1088/1126-6708/2007/07/062 [arXiv:0705.0016 [hep-th]].
- [5] L. Amico, R. Fazio, A. Osterloh and V. Vedral, “Entanglement in many-body systems,” *Rev. Mod. Phys.* **80**, 517-576 (2008) doi:10.1103/RevModPhys.80.517 [arXiv:quant-ph/0703044 [quant-ph]].
- [6] T. Nishioka and T. Takayanagi, “AdS Bubbles, Entropy and Closed String Tachyons,” *JHEP* **01**, 090 (2007) doi:10.1088/1126-6708/2007/01/090 [arXiv:hep-th/0611035 [hep-th]].
- [7] Klebanov, I., Kutasov, D. & Murugan, A. “Entanglement as a probe of confinement,” *Nuclear Physics B* **796**, 274-293 (2008) doi:10.1016/j.nuclphysb.2007.12.017

- [8] A. Pakman and A. Parnachev, “Topological Entanglement Entropy and Holography,” *JHEP* **07**, 097 (2008) doi:10.1088/1126-6708/2008/07/097 [arXiv:0805.1891 [hep-th]].
- [9] X. X. Zeng and L. F. Li, “Holographic Phase Transition Probed by Nonlocal Observables,” *Adv. High Energy Phys.* **2016**, 6153435 (2016) doi:10.1155/2016/6153435 [arXiv:1609.06535 [hep-th]].
- [10] S. Mahapatra, “Interplay between the holographic QCD phase diagram and mutual $\&$ n -partite information,” *JHEP* **04**, 137 (2019) doi:10.1007/JHEP04(2019)137 [arXiv:1903.05927 [hep-th]].
- [11] G. Vidal and R. F. Werner, *Phys. Rev. A* **65**, 032314 (2002) doi:10.1103/PhysRevA.65.032314 [arXiv:quant-ph/0102117 [quant-ph]].
- [12] G. Vidal and R. F. Werner, “Computable measure of entanglement,” *Phys. Rev. A* **65** (2002), 032314 doi:10.1103/PhysRevA.65.032314 [arXiv:quant-ph/0102117 [quant-ph]].
- [13] M. B. Plenio, “Logarithmic negativity: a full entanglement monotone that is not convex,” *Physical review letters*, vol. 95, no. 9, p. 090503, 2005.
- [14] R. Horodecki, P. Horodecki, M. Horodecki and K. Horodecki, “Quantum entanglement,” *Rev. Mod. Phys.* **81** (2009), 865-942 doi:10.1103/RevModPhys.81.865 [arXiv:quant-ph/0702225 [quant-ph]].
- [15] Levin, Michael, and Xiao-Gang Wen. “Detecting topological order in a ground state wave function,” *Physical review letters* **96.11** (2006): 110405.
- [16] Q. Si and F. Steglich, “Heavy Fermions and Quantum Phase Transitions,” *Science* **329**, 1161 (2010) doi:10.1126/science.1191195 [arXiv:1102.4896 [cond-mat.str-el]].
- [17] A. C. Neto, “Charge density wave, superconductivity, and anomalous metallic behavior in 2d transition metal dichalcogenides,” *Physical review letters* **86**, (2001). doi:10.1103/PhysRevLett.86.4382
- [18] P. Gegenwart, Q. Si, and F. Steglich, “Quantum criticality in heavy-fermion metals,” *nature physics* **4**, 186–197 (2008) doi:10.1038/nphys892
- [19] K. I. Bolotin, F. Ghahari, M. D. Shulman, H. L. Stormer, and P. Kim, “Observation of the fractional quantum hall effect in graphene,” *nature* **462**, 196–199 (2009). doi:10.1038/nature08582
- [20] L. Susskind, “The World as a hologram,” *J. Math. Phys.* **36**, 6377-6396 (1995) doi:10.1063/1.531249 [arXiv:hep-th/9409089 [hep-th]].
- [21] J. M. Maldacena, “The Large N limit of superconformal field theories and supergravity,”

- Adv. Theor. Math. Phys. **2**, 231-252 (1998) doi:10.4310/ATMP.1998.v2.n2.a1 [arXiv:hep-th/9711200 [hep-th]].
- [22] P. Liu and J. P. Wu, “Mixed state entanglement and thermal phase transitions,” Phys. Rev. D **104** (2021) no.4, 046017 doi:10.1103/PhysRevD.104.046017 [arXiv:2009.01529 [hep-th]].
- [23] R. G. Cai, S. He, L. Li and Y. L. Zhang, “Holographic Entanglement Entropy on P-wave Superconductor Phase Transition,” JHEP **07** (2012), 027 doi:10.1007/JHEP07(2012)027 [arXiv:1204.5962 [hep-th]].
- [24] Y. Ling, P. Liu, C. Niu, J. P. Wu and Z. Y. Xian, “Holographic Entanglement Entropy Close to Quantum Phase Transitions,” JHEP **04**, 114 (2016) doi:10.1007/JHEP04(2016)114 [arXiv:1502.03661 [hep-th]].
- [25] Y. Ling, P. Liu and J. P. Wu, “Characterization of Quantum Phase Transition using Holographic Entanglement Entropy,” Phys. Rev. D **93**, no.12, 126004 (2016) doi:10.1103/PhysRevD.93.126004 [arXiv:1604.04857 [hep-th]].
- [26] P. Liu, C. Niu and J. P. Wu, “The Effect of Anisotropy on Holographic Entanglement Entropy and Mutual Information,” Phys. Lett. B **796**, 155-161 (2019) doi:10.1016/j.physletb.2019.07.035 [arXiv:1905.06808 [hep-th]].
- [27] G. Fu, P. Liu, H. Gong, X. M. Kuang and J. P. Wu, “Holographic informational properties for a specific Einstein-Maxwell-dilaton gravity theory,” Phys. Rev. D **104**, no.2, 026016 (2021) doi:10.1103/PhysRevD.104.026016 [arXiv:2007.06001 [hep-th]].
- [28] H. Gong, P. Liu, G. Fu, X. M. Kuang and J. P. Wu, “Informational properties of holographic Lifshitz field theory,” Chin. Phys. C **45**, no.6, 6 (2021) doi:10.1088/1674-1137/abefca [arXiv:2009.00450 [hep-th]].
- [29] P. Liu, Y. Ling, C. Niu and J. P. Wu, “Entanglement of Purification in Holographic Systems,” JHEP **09**, 071 (2019) doi:10.1007/JHEP09(2019)071 [arXiv:1902.02243 [hep-th]].
- [30] Y. f. Huang, Z. j. Shi, C. Niu, C. y. Zhang and **P. Liu**, “*Mixed State Entanglement for Holographic Axion Model*,” Eur. Phys. J. C **80**, no.5, 426 (2020) doi:10.1140/epjc/s10052-020-7921-y [arXiv:1911.10977 [hep-th]].
- [31] T. Takayanagi and K. Umemoto, “Entanglement of purification through holographic duality,” Nature Phys. **14**, no.6, 573-577 (2018) doi:10.1038/s41567-018-0075-2 [arXiv:1708.09393 [hep-th]].
- [32] K. Umemoto and Y. Zhou, “Entanglement of Purification for Multipartite States and its

- Holographic Dual,” JHEP **10**, 152 (2018) doi:10.1007/JHEP10(2018)152 [arXiv:1805.02625 [hep-th]].
- [33] S. Dutta and T. Faulkner, “A canonical purification for the entanglement wedge cross-section,” JHEP **03** (2021), 178 doi:10.1007/JHEP03(2021)178 [arXiv:1905.00577 [hep-th]].
- [34] J. Kudler-Flam and S. Ryu, “Entanglement negativity and minimal entanglement wedge cross sections in holographic theories,” Phys. Rev. D **99** (2019) no.10, 106014 doi:10.1103/PhysRevD.99.106014 [arXiv:1808.00446 [hep-th]].
- [35] N. Jokela and A. Pönni, “Notes on entanglement wedge cross sections,” JHEP **07** (2019), 087 doi:10.1007/JHEP07(2019)087 [arXiv:1904.09582 [hep-th]].
- [36] Y. Ling, P. Liu, Y. Liu, C. Niu, Z. Y. Xian and C. Y. Zhang, “Reflected entropy in double holography,” JHEP **02**, 037 (2022) doi:10.1007/JHEP02(2022)037 [arXiv:2109.09243 [hep-th]].
- [37] C. Y. Chen, W. Xiong, C. Niu, C. Y. Zhang and P. Liu, “Entanglement wedge minimum cross-section for holographic aether gravity,” JHEP **08** (2022), 123 doi:10.1007/JHEP08(2022)123 [arXiv:2109.03733 [hep-th]].
- [38] Z. Yang, F. J. Cheng, C. Niu, C. Y. Zhang and P. Liu, “The mixed-state entanglement in holographic p-wave superconductor model,” JHEP **04**, 110 (2023) doi:10.1007/JHEP04(2023)110 [arXiv:2301.13574 [hep-th]].
- [39] P. Liu, C. Niu, Z. J. Shi and C. Y. Zhang, “Entanglement wedge minimum cross-section in holographic massive gravity theory,” JHEP **08**, 113 (2021) doi:10.1007/JHEP08(2021)113 [arXiv:2104.08070 [hep-th]].
- [40] C. Y. Chen, M. J. Li, Z. Yang, D. M. Jin and P. Liu, “Diagnosing Emergent Isotropy in Anisotropic Holographic Systems using Quantum Information Measures,” [arXiv:2404.11021 [hep-th]].
- [41] P. Liu, Z. Yang, C. Niu, C. Y. Zhang and J. P. Wu, “Mixed-state entanglement for AdS Born-Infeld theory,” JHEP **09**, 105 (2023) doi:10.1007/JHEP09(2023)105 [arXiv:2301.04854 [hep-th]].
- [42] M. J. Li, C. Y. Chen, C. Niu, C. Y. Zhang and P. Liu, “Mixed-state entanglement and transport in Einstein–Maxwell–Axion–Horndeski theory,” Eur. Phys. J. C **84**, no.2, 164 (2024) doi:10.1140/epjc/s10052-024-12521-2 [arXiv:2311.01172 [hep-th]].
- [43] D. A. Roberts and B. Swingle, “Lieb–Robinson Bound and the Butterfly Effect in Quantum Field Theories,” Phys. Rev. Lett. **117**, no.9, 091602 (2016)

doi:10.1103/PhysRevLett.117.091602 [arXiv:1603.09298 [hep-th]].

- [44] S. H. Shenker and D. Stanford, “Black holes and the butterfly effect,” *JHEP* **03**, 067 (2014) doi:10.1007/JHEP03(2014)067 [arXiv:1306.0622 [hep-th]].
- [45] M. Blake, “Universal Charge Diffusion and the Butterfly Effect in Holographic Theories,” *Phys. Rev. Lett.* **117**, no.9, 091601 (2016) doi:10.1103/PhysRevLett.117.091601 [arXiv:1603.08510 [hep-th]].
- [46] P. Liu and J. P. Wu, “Dynamic properties of two-dimensional latticed holographic system,” *JHEP* **02**, 119 (2022) doi:10.1007/JHEP02(2022)119 [arXiv:2104.04189 [hep-th]].
- [47] Y. Ling, P. Liu and J. P. Wu, “Holographic Butterfly Effect at Quantum Critical Points,” *JHEP* **10**, 025 (2017) doi:10.1007/JHEP10(2017)025 [arXiv:1610.02669 [hep-th]].
- [48] Y. Ling, P. Liu and J. P. Wu, “Note on the butterfly effect in holographic superconductor models,” *Phys. Lett. B* **768**, 288-291 (2017) doi:10.1016/j.physletb.2017.03.010 [arXiv:1610.07146 [hep-th]].
- [49] W. Xiong, P. Liu, C. Niu, C. Y. Zhang and B. Wang, “Dynamical spontaneous scalarization in Einstein-Maxwell-scalar theory *,” *Chin. Phys. C* **46**, no.9, 095103 (2022) doi:10.1088/1674-1137/ac70ad [arXiv:2205.07538 [gr-qc]].
- [50] C. Y. Zhang, P. Liu, Y. Liu, C. Niu and B. Wang, “Dynamical charged black hole spontaneous scalarization in anti-de Sitter spacetimes,” *Phys. Rev. D* **104**, no.8, 084089 (2021) doi:10.1103/PhysRevD.104.084089 [arXiv:2103.13599 [gr-qc]].
- [51] J. Eisert, M. Cramer and M. B. Plenio, “Area laws for the entanglement entropy - a review,” *Rev. Mod. Phys.* **82** (2010), 277-306 doi:10.1103/RevModPhys.82.277 [arXiv:0808.3773 [quant-ph]].
- [52] Nielsen, Michael A. and Chuang, Isaac L., “Quantum Computation and Quantum Information: 10th Anniversary Edition,” Cambridge: Cambridge University Press (2010). doi:10.1017/CBO9780511976667
- [53] H. B. Zeng, X. Gao, Y. Jiang and H. S. Zong, “Analytical Computation of Critical Exponents in Several Holographic Superconductors,” *JHEP* **05** (2011), 002 doi:10.1007/JHEP05(2011)002 [arXiv:1012.5564 [hep-th]].
- [54] Q. Pan, J. Jing, B. Wang and S. Chen, “Analytical study on holographic superconductors with backreactions,” *JHEP* **06** (2012), 087 doi:10.1007/JHEP06(2012)087 [arXiv:1205.3543 [hep-th]].

- [55] N. Bao and I. F. Halpern, JHEP **03** (2018), 006 doi:10.1007/JHEP03(2018)006 [arXiv:1710.07643 [hep-th]].
- [56] C. Y. Zhang, C. Niu, W. L. Qian, X. Wang and P. Liu, “Traversable thin-shell wormhole in the 4D Einstein–Gauss–Bonnet theory,” Chin. J. Phys. **83**, 527-538 (2023) doi:10.1016/j.cjph.2023.04.016 [arXiv:2004.14267 [gr-qc]].
- [57] P. Liu, C. Niu and C. Y. Zhang, “Instability of regularized 4D charged Einstein-Gauss-Bonnet de-Sitter black holes,” Chin. Phys. C **45**, no.2, 025104 (2021) doi:10.1088/1674-1137/abcd2d [arXiv:2004.10620 [gr-qc]].
- [58] P. Liu, C. Niu and C. Y. Zhang, “Linear instability of charged massless scalar perturbation in regularized 4D charged Einstein-Gauss-Bonnet anti de-Sitter black holes,” Chin. Phys. C **45**, no.2, 025111 (2021) [arXiv:2005.01507 [gr-qc]].
- [59] A. Donos and J. P. Gauntlett, “Holographic Q-lattices,” JHEP **04** (2014), 040 doi:10.1007/JHEP04(2014)040 [arXiv:1311.3292 [hep-th]].
- [60] K. Landsteiner, Y. Liu and Y. W. Sun, “Quantum phase transition between a topological and a trivial semimetal from holography,” Phys. Rev. Lett. **116** (2016) no.8, 081602 doi:10.1103/PhysRevLett.116.081602 [arXiv:1511.05505 [hep-th]].
- [61] Y. Ling, P. Liu, J. P. Wu and Z. Zhou, “Holographic Metal-Insulator Transition in Higher Derivative Gravity,” Phys. Lett. B **766** (2017), 41-48 doi:10.1016/j.physletb.2016.12.051 [arXiv:1606.07866 [hep-th]].
- [62] M. Baggioli, B. Padhi, P. W. Phillips and C. Setty, “Conjecture on the Butterfly Velocity across a Quantum Phase Transition,” JHEP **07**, 049 (2018) doi:10.1007/JHEP07(2018)049 [arXiv:1805.01470 [hep-th]].
- [63] M. Baggioli and D. Giataganas, “Detecting Topological Quantum Phase Transitions via the c-Function,” Phys. Rev. D **103**, no.2, 026009 (2021) doi:10.1103/PhysRevD.103.026009 [arXiv:2007.07273 [hep-th]].
- [64] Y. Ling, P. Liu and J. P. Wu, “A novel insulator by holographic Q-lattices,” JHEP **02**, 075 (2016) doi:10.1007/JHEP02(2016)075 [arXiv:1510.05456 [hep-th]].
- [65] Y. Ling, P. Liu, C. Niu and J. P. Wu, “Building a doped Mott system by holography,” Phys. Rev. D **92**, no.8, 086003 (2015) doi:10.1103/PhysRevD.92.086003 [arXiv:1507.02514 [hep-th]].
- [66] Y. Ling, P. Liu, C. Niu, J. P. Wu and Z. Y. Xian, “Holographic fermionic system with dipole coupling on Q-lattice,” JHEP **12**, 149 (2014) doi:10.1007/JHEP12(2014)149 [arXiv:1410.7323

[hep-th]].